A direct and versatile assay measuring membrane penetration of adenovirus in single cells

Suomalainen, Maarit ; Luisoni, Stefania ; Boucke, Karin ; Bianchi, Sarah ; Engel, Daniel A ; Greber, Urs F

Abstract: Endocytosis is the most prevalent entry port for viruses into cells, but viruses must escape from the lumen of endosomes to ensure that viral genomes reach a site for replication and progeny formation. Endosomal escape also helps viruses bypass endo-lysosomal degradation and presentation to certain toll-like intrinsic immunity receptors. The mechanisms for cytosolic delivery of non-enveloped viruses or nucleocapsids from enveloped viruses are poorly understood, in part because no quantitative assays are readily available, which directly measure the penetration of viruses into the cytosol. Following uptake by clathrin-mediated endocytosis or macropinocytosis, the non-enveloped adenoviruses penetrate from endosomes to the cytosol, and they traffic with cellular motors on microtubules to the nucleus for replication. In this study, we present a novel single cell imaging assay, which quantitatively measures individual cytosolic viruses and distinguishes them from endosomal viruses or viruses at the plasma membrane. Using this assay, we show that the penetration of human adenoviruses from the species C and B occurs rapidly after virus uptake. Efficient penetration does not require acidic pH in endosomes. This assay is versatile, and can be adapted to other adenoviruses, and members of other non-enveloped and enveloped virus families.

DOI: https://doi.org/10.1128/JVI.01833-13

A direct and versatile assay measuring membrane penetration of adenovirus in single cells

Maarit Suomalainen[2], Stefania Luisoni[2,3], Karin Boucke[2], Sarah Bianchi[2*], Daniel A. Engel[4] and Urs F. Greber[1, 2]

[1] corresponding author: urs.greber@imls.uzh.ch

[2] Institute of Molecular Life Sciences, University of Zurich, Zurich, Switzerland

[3] Molecular Life Sciences Graduate School, ETH and University of Zurich, Switzerland

[4] Department of Microbiology, Immunology and Cancer Biology, University of Virginia School of Medicine, Charlottesville, VA, USA

*Present address: Paul Scherrer Institute, Villigen, Switzerland

Keywords:

Membrane penetration, endosomal lysis, cytosolic escape, single virus fluorescence microscopy, low pH, endosome, virus entry, trafficking

Running title:
Light microscopy decodes cytosolic / endosomal viruses

Word count:
Abstract: 193
Text (excl refs, fig legends):

Abstract

Endocytosis is the most prevalent entry port for viruses into cells, but viruses must escape from the lumen of endosomes to ensure that viral genomes reach a site for replication and progeny formation. Endosomal escape also helps viruses bypass endo-lysosomal degradation and presentation to certain toll-like intrinsic immunity receptors. The mechanisms for cytosolic delivery of non-enveloped viruses or nucleocapsids from enveloped viruses are poorly understood, in part because no quantitative assays are readily available, which directly measure the penetration of viruses into the cytosol. Following uptake by clathrin-mediated endocytosis or macropinocytosis, the non-enveloped adenoviruses penetrate from endosomes to the cytosol, and they traffic with cellular motors on microtubules to the nucleus for replication. In this study, we present a novel single cell imaging assay, which quantitatively measures individual cytosolic viruses and distinguishes them from endosomal viruses or viruses at the plasma membrane. Using this assay, we show that the penetration of human adenoviruses from the species C and B occurs rapidly after virus uptake. Efficient penetration does not require acidic pH in endosomes. This assay is versatile, and can be adapted to other adenoviruses, and members of other non-enveloped and enveloped virus families.

Introduction

Cell entry of viruses involves crossing of the plasma membrane, or an endosomal membrane following endocytic uptake. In fact, endocytosis is the major pathway for virus infections (for recent reviews, see 1, 2-5). Enveloped viruses are well known to fuse their lipid membrane with the plasma membrane or the endosomal membrane, and thereby deliver their internal core structures into the cytoplasm. In contrast, the membrane penetration of non-enveloped viruses is less well understood, but equally important, since it gives rise to cytosolic viruses which are sensed by intrinsic and innate host defense systems (for reviews, see 6, 7). Central to non-enveloped virus penetration is a virally encoded membrane lytic factor, which either forms a pore on the limiting membrane, causes disintegration, or locally modifies the host membrane composition (reviewed in, 8, 9). This eventually enables the viral capsid to traverse the membrane barrier and access the cytosol. In intact non-enveloped viruses the membrane lytic factor is internal and its exposure requires a metastable capsid structure that can undergo structural rearrangements in response to cellular cues. The precise molecular mechanisms by which these membrane lytic factors bring about the virus penetration, or the host components that participate in the process, are poorly characterized. One issue that has hampered the progress is the lack of suitable assays that can quantitatively and directly measure virus penetration efficiency in infected cells.

Human adenoviruses are non-enveloped icosahedral viruses, replicating in the cell nucleus with lytic release of progeny to the medium (10). They are classified into seven species (HAdV-A to G, 11). The ~90nm outer capsid shell is formed by the major structural protein hexon and stabilized by minor cementing proteins (12, 13). Proteolytic processing of the cementing proteins by a virion-associated protease converts the capsid into a metastable structure that is capable of undergoing a stepwise uncoating during entry, and successful delivery of the viral genome into the nucleus (14-16). Attachment and uptake of adenoviruses into cells are mediated by vertex-associated fiber and penton base proteins, respectively, after a distinct series of motion steps on the cell surface (17). Coxsackievirus adenovirus receptor (CAR)

is the primary attachment receptor for species C adenoviruses, such as HAdV-C2 and HAdV-C5 (18, 19), whereas integrins αvβ3 and αvβ5 mediate virus uptake via clathrin-mediated endocytosis (20-24). In contrast, species B viruses bind to cells via CD46 or desmoglein 2 (25, 26), and are internalized by macropinocytosis (27, 28). Following internalization, HAdV-C2/C5 viruses penetrate into the cytosol from an as-yet-unidentified early endosomal compartment (15, 20), whereas penetration of species B adenoviruses has been postulated to occur from late endosomes (29).

Escape of incoming adenoviruses from endosomes is dependent on the viral membrane lytic protein VI (30, 31). To expose protein VI from the inside of the virus, the virus uses CAR to engage in actomyosin-2-dependent drifting motions on the cell surface, and uses integrin binding for confinement (32). These two counteracting motions lead to a mechanical strain that releases fibers and causes structural changes in the particle that enable efficient exposure of protein VI (32). The escape of HAdV-C2/5 is apparently mediated by protein VI-induced disruption of an endosomal membrane, since HAdV-C2/C5 can promote delivery of co-internalized 70-kDa dextran, 25 nm parvovirus particles or membrane-impermeable bacterial toxins into the cytosol (31, 33-35). Furthermore, recombinant protein VI fragments liposomes *in vitro* (30). Critical for membrane disruption is an N-terminal amphipathic α-helix in protein VI (30, 31, 36, 37). In HAdV-C2_TS1 mutant virus (TS1) the capsid cementing proteins are unprocessed due to a point mutation in the viral protease (16). This mutant virus is unable to undergo structural changes that enable penetration during entry, and the virus particles end up trapped in late endosomes/lysosomes (14, 20, 32, 38).

A controversial question in the penetration of HAdV-C2/C5 viruses has been the role of acidic endosomal pH. Although *in vitro* studies have shown that acidic pH can destabilize the virion structure and promote protein VI exposure (30, 39), fragmentation of liposomes by recombinant protein VI is a pH-independent reaction (30). Furthermore, delivery of co-internalized dextran into the cytosol in HAdV-C5 infected cells has been reported to be unaffected by neutralization of endosomal pH by the vacuolar H^+-ATPase inhibitor bafilomycin A1 (33). On the other hand,

inhibition of endosomal acidification has been reported to reduce cytosolic delivery of co-internalized bacterial toxins (35, 40, 41), and overall viral infection efficiency (15, 42). However, none of these studies directly monitored cytosolic and endosomal virus populations in the infected cells. Here we report a single cell based imaging assay for direct quantification of cytosolic and endosomal viruses during entry into cells. Our results indicate that incoming HAdV-C2/C5 particles rapidly and efficiently escape from endosomes, and that efficient membrane penetration does not require acidic endosomal pH. The assay is easily adapted to other adenoviruses, as exemplified by HAdV-B3, and potentially also to other non-enveloped viruses.

Materials and Methods

Cells and viruses

HeLa cervical carcinoma cells, subline Ohio (from L. Kaiser, University Hospital, Geneva, Switzerland) (43), human bronchial epithelial A549 cells and human embryonic retinoblast 911 cells were grown at 37°C under 5% CO_2 in Dulbecco's modified Eagle's medium (DMEM, Sigma) supplemented with 7.5 % FCS (Life Technologies) and 1% nonessential amino acids (Sigma). Human adenoviruses HAdV-C2, the penetration deficient mutant HAdV-C2_TS1, HAdV-C5 and HAdV-B3 were grown in A549 cells, isolated and labeled with Alexa Fluor 488 (Alexa-488, Life Technologies) or atto-565 (Atto-tec, Germany) as previously described (14, 15, 44). HAdV-C5_EGFP, an E1/E3 deleted mutant virus containing EGFP gene in the E1 region under the control of cytomegalovirus major immediate early promoter (45, 46), as well as the EGFP-expressing, non-replicating HAdV-B3_EGFP virus (47), were grown in 911 cells.

Streptolysin O (SLO)-penetration assay

HeLa-Ohio or A549 cells were seeded on Alcian blue-coated glass coverslips (48) in 24-well dishes (40000 cells / well) and grown for 2 days. Alexa-488-labeled viruses (~0.5µg virus/well yielding about 10-200 bound particles/cell) were bound to cells at 0°C for 60 min in RPMI-1640 medium (without $NaHCO_3$, Sigma) supplemented with 0.2% bovine serum albumin (BSA), 20mM Hepes and penicillin/streptomycin (=RPMI-BSA medium). The unbound virus was washed away and the cells in RPMI-BSA medium were placed into a 37°C water bath. After virus internalization, cells were placed on ice, washed twice with SLO-binding buffer (25 mM Hepes-KOH pH 7.4, 110 mM potassium acetate, 2.5 mM magnesium acetate, 0.2 mM calcium chloride, 1 mM EGTA, 1 mM DTT) and processed for Streptolysin O (SLO)-mediated perforation of the plasma membrane. SLO was kindly provided by M. Husmann and S. Bhakdi (University Medical Center, Johannes Gutenberg-University Mainz), or, alternatively, purchased from Sigma. The SLO was pre-activated in SLO-binding buffer at room temperature (RT) for 5 min, just before use. The activated SLO was applied to cells in ice-cold SLO binding buffer and bound to the cell plasma membrane on ice for 10 min. The unbound SLO was washed away, and cells in

SLO-binding buffer were switched to a 37°C water bath for 5 min to allow oligomerization of SLO and pore formation. The exact amount of SLO needed to permeabilise the cells varied between 0.4-3 µg per well depending on the SLO batch. After the pore formation step, cells were placed back on ice, washed twice with antibody-incubation buffer (25mM Hepes-KOH pH 7.4, 110 mM potassium acetate, 2.5 mM magnesium acetate, 2 mM EGTA), and incubated with rabbit anti-Alexa-488 antibody (Life Technologies: antibody diluted in the antibody-incubation buffer) on ice for 60 min. Unbound antibody was washed away, cells were fixed with 3% paraformaldehyde (prepared in 25mM Hepes-KOH pH 7.4, 110 mM potassium acetate, 2.5 mM magnesium acetate) at RT for 20 min, quenched for 10 min with 25 mM ammonium chloride in PBS, and permeabilised with 0.5% Triton X-100 in PBS at RT for 5min. Cells were blocked with 10% goat serum, and stained with goat Alexa Fluor 594 (Alexa-594)-conjugated anti-rabbit antibodies (Life Technologies), and with DAPI to identify the nuclei. Intact cells incubated with anti-Alexa-488 antibodies in RPMI-BSA medium for 1h on ice were used to estimate the number of plasma membrane-associated viruses. SLO-treated samples fixed and permeabilised with Triton X-100 before the addition of anti-Alexa-488 antibodies (so called TX-100 samples) were used to control the overall accessibility of the internalized virus for the antibodies. The samples were imaged with Leica SP5 confocal laser scanning microscope using 63 × objective (oil immersion, numerical aperture 1.4) and zoom factor 2. Excitations were at 405 nm (DAPI), 488 nm (virus) and 561 or 594 nm [antibody signal; excitation was at 633 nm if Alexa Fluor 633 (Alexa-633) or Alexa Fluor 680 (Alexa-680) secondary antibodies were used]. Stacks were recorded at 0.5 µm intervals using 4 × averaging and sequential acquisition for the individual channels. Maximum projections of confocal stacks were analyzed by a custom programmed MatLab (The Mathworks) routine to score individual virus particles within single cells and to quantify the anti-Alexa-488 antibody signal on the particles (49). The MatLab routines used in this study will be made available upon request. The threshold value for positive antibody signal was determined by placing a virus image on an antibody image obtained from non-infected cells and taking the highest virus-associated antibody signal as a cut-off value. As with any thresholds, classification mistakes may occur due to particles that have values close to the threshold. With our procedure, less than 3.5% of particles had values within 20% of the threshold value (see for example Fig. 1D), indicating that the thresholding errors

are small. Further, over 95% of viruses in the TX-100 samples had an anti-Alexa-488 signal higher than the threshold value indicating that this thresholding procedure efficiently detected most of the viruses. Representative images shown in figures were processed with Image J applying the same changes in brightness and contrast to all image groups in the series (http://rsbweb.nih.gov/ij/).

For wild type (wt) HAdV-C2 and TS1 virus coinfection, unlabeled wt and Alexa-488-labeled TS1 were bound to HeLa-Ohio cells at cold to synchronize the infection, and subsequently internalized at 37°C for 30 min before permeabilization with SLO as described above. Mean number of bound wt viruses per cell was 99, and 40 for TS1. The wt and TS1 viruses in the SLO-treated cells were detected with mouse anti-hexon 9C12 antibody (50) and anti-Alexa-488 antibody, respectively. Secondary antibodies were Alexa-680-conjugated goat anti-mouse and Alexa-594-conjugated goat anti-rabbit, respectively. The 9C12 antibody, developed by Laurence Fayadat and Wiebe Olijve, was obtained from Developmental Studies Hybridoma Bank developed under the auspices of the NICHD and maintained by the University of Iowa, Department of Biology, Iowa City, IA 52242.

Simultaneous detection of surface, endosomal and cytosolic viruses in cells infected with Alexa-488-labeled wild type HAdV-C5 was carried out by first incubating intact cells with anti-hexon 9C12 antibody in RPMI-BSA medium for 1h on ice. After removing unbound antibodies, cells were permeabilized with SLO and incubated with anti-Alexa-488 antibodies as described above. Secondary antibodies were Alexa-633-conjugated anti-rabbit and Alexa-594-conjugated anti-mouse. Particles that scored positive for 9C12 antibody were classified as surface viruses, and particles that were 9C12-negative, but anti-Alexa-488-positive were classified as cytosolic viruses. Single antibody stainings were used to control that there were no signal spillover artefacts.

To determine the effect of endosome neutralization on virus penetration, the cells were pre-incubated with Bafilomycin A1 (Baf A1, Sigma, 50 nM in growth medium), niclosamide (Sigma, 5 μM in plain RPMI-1640 medium, 51) and NH_4Cl (25mM in

RPMI-BSA pH 8.2 medium) for 1h before the virus addition. Control cells were treated with dmso (Baf A1 and niclosamide) or the pH 8.2 RPMI-BSA medium (NH_4Cl). The assay was carried out as described above, except that virus binding and internalization were in media containing the drugs. To control the effectiveness of the drugs and NH_4Cl, cells were incubated in RPMI-BSA medium containing 2 μM Lysotracker DND-99 (Life Technologies) at RT for 15 min after the drug pretreatment, washed twice with PBS and fixed with 3% paraformaldehyde containing 3 μg/ml Hoechst 33342 (Sigma).

EM assay for penetration

HeLa-Ohio cells grown on Alcian blue-coated glass coverslips were pretreated with dmso (control), Baf A1 or niclosamide for 1h as described above. Fifteen μg of HAdV-C2 was bound to cells at cold and the virus was internalized at 37°C for 30 min in the presence of dmso or the drugs. Samples were processed for electron microscopy as previously described (20). For quantification, digital micrographs were recorded in sections across the middle of the cells imaged at 50000x magnification as described (52). The number of viruses at the plasma membrane, in endosomes and the cytosol was determined by manual counting.

Assay for protein VI exposure

HeLa-Ohio cells grown on Alcian blue-coated glass coverslips were pretreated with Baf A1, niclosamide or ammonium chloride for 1 h as described above, and the drugs were present in the medium throughout the experiment. Atto565-labeled HAdV-C5 was bound to cells at cold, and internalized at 37°C for indicated times. After internalization, intact cells were incubated with the 9C12 anti-hexon antibody on ice to tag virus particles at the cell surface. Cells were fixed with 3% paraformaldehyde and processed for anti-protein VI staining (see above, and 32). Alexa-680-conjugated goat anti-mouse and Alexa-488-conjugated goat anti-rabbit were used as secondary antibodies. The samples were imaged as described above. A custom programmed MatLab routine was used to quantify protein VI signal on endocytosed viruses, that is, Alexa-565-positive, but Alexa-680-negative viruses.

Assay for incoming nuclear protein VII

HeLa-Ohio cells grown on Alcian blue-coated glass coverslips were pretreated with dmso, Baf A1 or niclosamide for 1h as described above. HAdV-C5 was bound to cells at 37°C for 30 min in the presence of dmso or drugs, after which virus inoculum was removed and cells were either fixed with 3% paraformaldehyde (30 min sample) or further incubated at 37°C for 2.5 h in the presence of dmso or drugs before fixation (2.5 h sample). The samples were processed for immunofluorescence as described above. Anti-hexon 9C12 and Alexa-488-conjugated goat anti-mouse antibodies were used to estimate the number of virus particles bound per cell (30 min sample), and rabbit anti-protein VII (53) and Alexa-488-conjugated goat anti-rabbit antibodies were used to visualize nuclear protein VII dots in the 2.5 h sample. DAPI was used to mark the nuclear area. Cells were imaged as described above. Number of viruses per cell was analyzed by a custom programmed MatLab routine from maximum projections of confocal stacks, and the number of nuclear protein VII dots was analyzed by CellProfiler (http://cellprofiler.org).

Infection assays

To determine the effect of Baf A1 on virus infection, HeLa-Ohio cells grown on 96-well imaging plates (Greiner Bio-one) were pretreated with Baf A1 or dmso for 60 min as described above. HAdV-C5_EGFP or HAdV-B3_EGFP virus was bound to cells at 37°C for 30 min, after which virus inocula were removed and cells further incubated at 37°C for 17-18 h in growth medium containing dmso/Baf A1. Alternatively, dmso/Baf A1 were added 2 h after removal of virus inocula. The samples were fixed, processed and imaged as described (32). DAPI stain was used to mark the nuclear area, and custom programmed MatLab routine was used to determine the average nuclear intensity of the EGFP signal, which was taken as a measure of infection efficiency. To determine the effect of niclosamide on virus infection, HeLa-Ohio cells grown on 96-well imaging plates were pretreated with niclosamide or dmso for 60 min as described above, HAdV-C5_EGFP or HAdV-B3_EGFP virus was then bound to cells at 37°C for 30 min, after which virus inocula were removed and cells further incubated at 37°C for 3.5 h in the presence of

dmso/niclosamide, followed by 13-14.5 h incubation in a drug-free growth medium. Cells were processed and analyzed as described for the Baf A1 experiment.

Results

Endocytosed HAdV-C2 rapidly escapes from endosomes

Previous studies have suggested that species C human adenoviruses, such as HAdV-C2 and HAdV-C5, escape from early endosomes by causing disruption of the endosomal membrane (15, 20, 30). To quantitatively monitor the escape at single-cell level, we developed the assay outlined in Fig. 1A. The assay uses Alexa-488-labeled viruses, anti-Alexa-488 antibodies and the bacterial toxin Streptolysin O (SLO) (54). Virus particles are first bound to cells at cold to synchronize infection and cells are then switched to 37°C for virus internalization. After internalization, the plasma membrane of the infected cells is perforated by SLO. This allows access of anti-Alexa-488 antibodies into the cytosol and decoration of cytosolic viruses by the antibodies. In contrast, virus in endosomes is not accessible to the antibodies. Incubation of the permeabilised cells with antibodies is done at cold in a buffer devoid of ATP to suppress penetration of virus after SLO-permeabilization. After the primary antibody treatment, cells are fixed, permeabilised and stained with secondary Alexa-594-conjugated antibodies, and imaged by confocal microscopy. Cytosolic virus particles are recognized by the dual Alexa-488 and Alexa-594 signals, whereas endosomal viruses have only the Alexa-488 signal. Since viruses at the cell surface are also accessible to antibodies, the assay includes control samples stained with anti-Alexa-488 antibodies without prior SLO-permeabilization. Fig. 1B shows representative confocal images of HeLa-Ohio cells infected with Alexa-488-labeled wt HAdV-C2 or the penetration-deficient TS1 virus. The majority of wt particles were accessible to the anti-Alexa-488 antibodies 30 min post infection (pi), unlike TS1. Following uptake, TS1 particles are transported to late endosomes (20), and this explains the clustering of TS1 (Fig. 1B).

To determine the kinetics and efficiency of wt virus penetration, HeLa-Ohio cells infected with Alexa-488-labeled wt HAdV-C5 were analyzed at 0, 5, 10 or 20 min

after virus internalization. Intact cells were first stained with mouse anti-hexon 9C12 antibody, then permeabilized with SLO and incubated with the rabbit anti-Alexa-488 antibodies. After fixation, cells were permeabilized and stained with secondary Alexa-594-conjugated anti-mouse and Alexa-633-conjugated anti-rabbit antibodies, and imaged by confocal microscopy (Fig. 1C). Particles positive for 9C12 were classified as surface particles, and particles negative for 9C12, but positive for anti-Alexa-488 antibodies were classified as cytosolic viruses. Surface stains at the 0 min time point indicated that Alexa-488-labeled HAdV-C5 was efficiently recognized by both antibodies. After 5 min, about 47% of particles were at the cell surface and 39% in the cytosol. The surface population decreased to 13% and 1% at the 10 min and 20 min points in time, respectively, and the cytosolic population increased to 67% and 79%, respectively. Note that the size of surface and cytosolic virus populations varied considerably from cell-to-cell at 5 min and 10 min post internalization. Since the endosomal virus population at any of the time points amounted only to maximum of about 20%, this suggests that HAdV-C5 rapidly penetrates after endocytosis.

A time course was done with TS1-infected cells (Fig. 1D). Unfortunately, we could not score surface, endosomal and cytosolic viruses within the same cell, since TS1 is not recognized by the 9C12 antibody. Instead, intact cells stained with anti-Alexa-488 antibodies were used to estimate the size of surface virus population. Parallel SLO-permeabilized samples were stained with the same antibody to estimate the size of the cytosolic virus population. Significantly, the percentage of TS1 particles positive for anti-Alexa-488 antibody was similar in the 5 min surface and SLO-treated samples. Since the endocytosed TS1 particles at this time point are expected to be in early endosomes (20), this result indicates that early endosomes remain intact in the SLO-treated samples. Also the integrity of late endosomes appeared not to be compromised in the SLO-treated samples, since the vast majority of TS1 particles were not accessible to anti-Alexa-488 antibodies after 30 min of internalization, a time point when viruses have reached the late endosomes (20). TS1 virus preparations always contain some wt-like, penetration competent particles. A previous transmission-EM study estimated that 14% of incoming TS1 particles were found in the cytosol at 30 min post internalization (16). The 10% mean penetration efficiency of TS1 at 30 min post internalization in the present study agrees well with

these previous results. If SLO-perforated TS1-infected cells were fixed and permeabilised with Triton X-100 prior to staining with anti-Alexa-488 antibodies, then all TS1 particles became decorated with the antibody (Fig. 1D).

We next tested the penetration efficiency of TS1 in HAdV-C5 (wt) and TS1 co-infected cells to test the possibility that wt infection generally destabilized endosomes in the SLO-permeabilised cells. Unlabeled HAdV-C5 and Alexa-488-labeled TS1 particles were bound to HeLa-Ohio cells at cold and cells were permeabilised with SLO 30 min pi. As shown in Fig. 1E, HAdV-C5 particles were readily accessible to antibodies in the SLO-permeabilised cells. More TS1 particles were antibody-positive in cells co-infected with HAdV-C5 than in the single TS1 infection (3% compared to 8.5%), and the difference was statistically highly significant ($P<0.0001$, two-tailed Mann-Whitney test). Previous results from our laboratory indicated that maximally 7.5% of incoming HAdV-C2 co-localized with the early endosomal marker EEA1, and that 65% of HAdV-C2-positive early endosomes were also positive for TS1 in wt and TS1 co-infected cells (20). Thus wt virus is expected to enhance cytosolic delivery of TS1 in a co-infection situation, and this most likely explains the differences between TS1 single and wt-TS1 co-infections in Fig.1E. Notably, the overall number of antibody-positive TS1 particles in the co-infection was low in comparison to wt virus infections. The data thus indicate that wt virus infection does not lead to nonspecific disruptions of endosomes in presence of SLO.

So far, the experiments were done in HeLa-Ohio cells. We next tested the assay in A549 cells using Alexa-488-labeled HAdV-C2 (wt) or TS1 (Fig. 2). Parallel intact or SLO-permeabilized cells were incubated with anti-Alexa-488 antibodies 20 min post virus internalization. A minor fraction of HAdV-C2 remained at the plasma membrane at this time point. The vast majority of HAdV-C2 in the SLO-treated cells was accessible to anti-Alexa-488 antibodies indicating rapid and efficient virus penetration in these cells as well. The differences of intact and SLO-treated TS1 samples were not statistically significant. Taken together, the results suggest that our assay allows quantitative assessments of cytosolic and endosomal virus

populations. The results demonstrate that endocytosed wt HAdV-C rapidly and efficiently penetrates into the cytosol.

Acidic endosomal pH is not required for efficient penetration of HAdV-C2

To neutralize endosomal compartments we used different compounds blocking low endosomal pH by three different modes of action, bafilomycin A1 (Baf A1) blocking the v-ATPase (55), niclosamide acting as a protonophore (51) and NH_4Cl acting as a lysosomotropic weak base (56, 57). HeLa-Ohio cells were preincubated with the drugs for 60 min prior to cold synchronized infection with Alexa-488-labeled HAdV-C2 or HAdV-C2_TS1. Control samples were treated with dmso (Baf A1 and niclosamide) or with pH 8.2 culture medium (NH_4Cl). As shown by the lysotracker DND99 stain, all three drugs efficiently neutralized acidic compartments in cells (Fig. 3A).

Baf A1 did not inhibit endocytosis of wt HAdV-C2, since in the majority of cells >95% virus particles were inaccessible to anti-Alexa-488 antibodies in intact cells (Fig. 3B). The percentage of penetrated HAdV-C2 in control SLO-permeabilised cells varied between 16.5-89.1% at 20 min pi (mean 64.4%). Although a greater number of cells displayed virus penetration efficiencies < 40% in the Baf A1-treated sample, the difference between control and Baf A1 samples was not statistically significant. The TS1 control indicated that endosomes remained intact in the SLO-permeabilised Baf A1 samples. A similar analysis for niclosamide treated cells 60 min pi showed that HAdV-C2 was efficiently endocytosed, and the drug did not compromise endosomal integrity, as indicated by the TS1 control (Fig. 3C). Although HAdV-C2 escaped from endosomes less efficiently in niclosamide-treated cells (P=0.0011, two-tailed Mann-Whitney test compared to the control cells), the mean penetration efficiency of HAdV-C2 was 63.2%, far higher than that of TS1. Similarly, the escape of wt virus to cytosol was significantly less efficient also in NH_4Cl treated cells than in control cells (Fig. 3D, 30 min pi), but again the overall penetration efficiency was relatively slightly affected, in agreement with Baf A1 or niclosamide treated cells. These results strongly suggest that acidic pH in endosomes is not needed for efficient penetration. This was in agreement with transmission-EM analyses 30 min post internalization.

No statistically significant differences were observed between control and Baf A1, or control and niclosamide samples (Fig. 3E and 3F).

We next analyzed the effect of Baf A1, niclosamide and NH_4Cl on exposure of the viral membrane lytic protein VI. As previously reported (32), protein VI is inaccessible to antibodies in intact virus particles (0 min sample, cold synchronized infection), but during early steps in the entry the virus undergoes structural changes that result in exposure of protein VI epitopes (Fig. 4A). Externalization of protein VI is a prerequisite for efficient penetration (32). HeLa-Ohio cells were pretreated with Baf A1, niclosamide or NH_4Cl for 1 h, atto-565-labeled HAdV-C5 was bound to cells at cold, and virus was internalized at 37°C (Fig. 4B-D). We restricted the analysis to endocytosed particles because protein VI exposure occurs concomitantly or soon after endocytosis (our unpublished observations). The average protein VI intensity on endocytosed particles in Baf A1 treated cells was slightly higher at 10 min pi than in control dmso treated cells (Fig. 4B). Protein VI separates from the virus particle following escape of the virus into the cytosol (32), and by 20min post internalization the protein VI intensity on endocytosed virions in Baf A1 and control samples was reduced to similar levels. No significant differences on protein VI signal on endocytosed particles were observed in control dmso or niclosamide treated cells at 10 min or 20 min pi (Fig. 4C). Similarly, NH_4Cl did not reduce protein VI exposure (Fig. 4D). Taken together, these results support the conclusion that acidic pH in endosomes is not needed for efficient penetration of HAdV-C.

Effect of endosome neutralization of nuclear import of protein VII and virus infection

We tested the effects of Baf A1 and niclosamide on entry steps downstream of penetration, such as nuclear targeting of the genome-associated protein VII 2.5 h pi (Fig. 5A, B, C). Low multiplicity of infection, resulting in 4-41 bound virus particles per cell was used in the assays, and Baf A1 and dmso treated cells bound virus with equal efficiency (Fig. 5A). As previously described (53, 58), incoming protein VII is seen as discreet dots over the nuclear area (Fig. 5B, nuclear area defined by DAPI signal). Quantification of protein VII dots per nucleus indicated that the number of

dots correlated with input virus, and similar numbers of dots were observed in dmso and Baf A1 treated cells (Fig. 5C). Nuclear targeting of protein VII was analyzed in niclosamide treated cells as well. Protein VII puncta in niclosamide treated cells were, however, less discrete and appeared to be more diffuse than in control cells, thus hindering accurate comparisons of the signals in these two samples (data not shown). Instead, we estimated the overall virus entry efficiency in Baf A1 or niclosamide treated cells by measuring the transgene expression from HAdV-C5-EGFP, a non-replicating, E1/E3-deleted virus (45). Surprisingly, Baf A1 treatment boosted infection efficiency by ~ 3.5-fold 17 h pi (Fig. 5D). However, this boost was not linked to penetration, since a significant increase in infection efficiency was also seen when Baf A1 was added 2h after removal of virus inoculum. Similar analyses of niclosamide treated cells showed that HAdV-C5-EGFP infection efficiency was ~76% of that in the control dmso cells (Fig. 5E). Collectively, the data demonstrate that acidic pH is not required for virus penetration to the cytosol and nuclear import of viral DNA-associated protein VII, but pH neutralization by Baf A1 increases transgene expression.

Acidic endosomal pH is not required for efficient penetration of HAdV-B3

Previous studies have shown that incoming HAdV-B traffic to late endosomes and lysosomes in larger extent than HAdV-C (29). We used Alexa-488-labeled HAdV-B3 as a model to monitor the kinetics of subgroup B virus escape from endosomes, and sensitivity of the escape to neutralization of endosomal pH. HeLa-Ohio cells were permeabilised by SLO at 30 min pi showing that a significant number of viruses had penetrated into the cytosol as evidenced by their accessibility to anti-Alexa-488 antibodies, but virus clusters that were negative for anti-Alexa-488 signal were observed as well (Fig. 6A, representative images). Quantitative assessment of uptake and escape showed that at 15 min pi, ~96% of viruses were endocytosed, and on average ~40% had penetrated into the cytosol (Fig. 6B). At 30 min pi, the penetration efficiency was not significantly different from that at 15 min pi, but considerable cell-cell variability in the penetration efficiency was observed, similar to HAdV-C. Similar to HAdV-C, Baf A1 did not inhibit endocytosis of HAdV-B3. Quantification of the Alexa-488 and Alexa-594 double positive particles indicated that HAdV-B3 penetrated as efficiently in the Baf A1-treated cells as in the control cells

(Fig. 6C). The difference in penetration efficiency of the virus in control compared to niclosamide treated cells was statistically significant, but the overall penetration efficiency was still high, even in the niclosamide sample (Fig. 6D). Taken together, these results demonstrate that acidic endosomal pH is not required for efficient penetration of HAdV-B3. We were not able to analyze effect of the drugs on HAdV-B3 protein VI exposure or protein VII nuclear import, since our antibodies did not react with HAdV-B3 (data not shown). Instead, we tested infection efficiency of a non-replicating HAdV-B3_EGFP virus in Baf A1-treated cells 18 h pi (47). If the drug was added 1h before the virus, ~4.6-fold boost in the infection efficiency was observed (Fig. 6E). The boost was significantly lower if the drug was added 2h after removal of the virus inoculum. A similar trend was observed in niclosamide treated cells (Fig. 6F). Thus, both Baf A1 and niclosamide boosted HAdV-B3-EGFP infection efficiency without having a large effect on the penetration step.

Discussion

In this study, we establish a new penetration assay for adenoviruses that quantitatively measures virus escape from endosomes at single-cell level. SLO-mediated perforation of the plasma membrane is used to introduce antibodies into the cytosol and accessibility of e.g. Alexa-488-labeled virus to anti-Alexa-488 antibodies distinguishes cytosolic from endosomal viruses in the permeabilised cells. Techniques such as delivery of co-internalized dextran or bacterial toxins into the cytosol by virus-induced rupture of endosomes (e.g., 33, 35, 40, 59, 60), or counting of viruses at the plasma membrane, endosomes and cytosol by EM (e.g., 27, 28, 61) have previously been used to estimate escape of HAdV-C and HAdV-B from endosomes. However, the co-delivery assays are bulk assays without single cell resolution, and most importantly these assays estimate virus penetration only indirectly. Furthermore, interpretation of the results from co-delivery assays can be complicated by the fact that HAdV-C induces macropinocytosis and leakage of macropinosomal contents into the cytosol (22, 27). This uptake pathway could be responsible for the delivery of bulk of the co-internalized dextran or bacterial toxins into the cytosol, but the macropinocytosis is not the infectious entry pathway at least for the HAdV-C (22). The EM assay on the other hand directly estimates cytosolic

and membrane-associated virus particles, but the assay is cumbersome and requires very high MOI.

The assay presented in this study can be used at high and low MOI. It is easy to set-up because the key components are commercially available - Alexa-488, anti-Alexa-488 antibody and SLO. However, there is one limiting factor, the choice of cell lines. Not all cells can endure the SLO permeabilisation, and some cell types detach from the dish, for example, U2OS cells. In this study, we used the HeLa-Ohio clone and A549 cells. In agreement with previous studies (e.g., 15, 29), we found that HAdV-C2 penetrates very rapidly after endocytic uptake. In a cold synchronized infection, a large fraction of viruses had escaped into the cytosol already 10 min after switching the cells to 37°C. Furthermore, the overall penetration efficiency was >60% at 20 min pi. Characterization of the early entry events for other adenovirus species is lagging behind that of HAdV-C. Our assay here is readily adaptable to other adenoviruses, as exemplified by HAdV-B3. We found that penetration of HAdV-B3 occurred rapidly, similar to HAdV-C2. At 15 min post internalization the overall escape efficiency was about 40%. The single cell resolution of our assay revealed considerable cell-to-cell variability in the virus penetration efficiency for both HAdV-C2 and HAdV-B3. While the molecular basis of this variability is currently unknown, it is interesting to note that the externalization of the viral membrane lytic protein VI to the surface of the virus also occurs with different efficiencies in individual cells.

There has been a long standing controversy regarding the role of acidic endosomal pH in adenovirus penetration (15, 30, 33, 40, 59, 62). Our escape assay indicated that efficient penetration of HAdV-C2 and HAdV-B3 occurs even if the pH in endosomes is neutralized. Furthermore, efficient exposure of the HAdV-C5 membrane lytic protein VI did not require acidic pH in endosomes. This was concluded from experiments using three distinct inhibitors to neutralize the endosomal pH: Baf A1 (vacuolar H^+-ATPase inhibitor), niclosamide (proton carrier) and ammonium chloride (lysomotropic weak base). Although the penetration of HAdV-C2 was affected to different degrees by these three treatments, the lysotracker control indicated that all three conditions efficiently neutralized acidic compartments

in the cell. The differences in penetration must hence be due to other effects of the compounds than endosomal pH neutralization. Interestingly, especially Baf A1 and ammonium chloride significantly reduced HAdV-C2 penetration in a subpopulation of the cells, suggesting that other endosomal factors than pH enhance HAdV penetration. Interestingly, a mild acid (pH 6) treatment of cells containing surface-bound HAdV-C2 increased the release of tritium labeled choline or ^{51}Cr from the cells compared to cells kept at neutral pH (62, 63). Possibly, low pH at the plasma membrane can substitute for an endosomal factor(s) in virus induced membrane perforation.

Although Baf A1 and niclosamide had relatively minor overall effects on the penetration efficiency of HAdV-C2 and HAdV-B3, a different picture emerged when the effect of these drugs was tested by EGFP-reporter viruses. In the case of HAdV-C5_EGFP virus, Baf A1 boosted infection efficiency by ~3.5-fold, whereas niclosamide reduced the infection by ~20%. In contrast, a significant infection boost was observed for HAdV-B3_EGFP virus, with both Baf A1 and niclosamide, possibly related to endosomal maturation which has been suggested to increase HAdV-C2 infection through autophagosome-endosome hybrid compartments (60). Regardless, the data highlight that it is crucial to employ direct assays for on-target interpretation of interference and perturbation experiments.

One intriguing observation in the current study was the rather low impact of co-internalized wt viruses on the penetration efficiency of the TS1 virus. The average penetration efficiency of TS1 in the co-infection was 8.5% and 3% in TS1 single infections. The TS1 virus escapes from endosomes inefficiently because it does not undergo the structural alterations that prepare the particle for efficient protein VI exposure (14, 32), but it interacts with CAR and integrins, and is internalized by clathrin-mediated endocytosis as the wt virus (20). HAdV-C2/C5 viruses penetrate from an as-yet-unidentified early endosomal compartment, since maturation of early endosomes to late endosomes is not required for efficient virus escape into the cytosol (20). The observed low impact of co-internalized wt particles on TS1 penetration could imply that the two viruses are sorted to different endosomal

compartments following uptake. Alternatively, the rapid penetration of wt virus may simply reduce co-localization of the two viruses in the same endosome compartment.

In summary, our study describes a quantitative single-cell assay for adenovirus escape from endosomes to the cytosol, a step that is poorly characterized at the molecular level. The assay can be used in combination with chemical inhibitors or possibly RNAi to probe for cellular regulators of the penetration step (64). Single-cell assays are important since it is becoming increasingly evident that cell-to-cell variation is observed in many cellular phenotypes, including virus entry (64). Correlation of virus entry and infection efficiencies with particular molecular or morphological properties of a single cell will give more accurate information about the molecular basis of a given event than an average phenotype acquired in a population assay. We expect that owing to its simplicity and reliability, the assay presented in this study also works for other non-enveloped viruses and even enveloped viruses, provided that they can be detected by an antibody in the selectively-permeabilised cells. Such an antibody can be directed against a viral nucleo-capsid protein or a chemical tag added to the virus, for example Alexa-488, as shown in this study for non-enveloped viruses.

Acknowledgments

We thank Martin Engelke, I-Hsuan Wang and Vibhu Prasad for MatLab scripts used in the study, and Robert Witte for help with CellProfiler analyses. This work was supported by grants from the Swiss National Science Foundation (SNF 31003A_141222/1 to UFG), SystemsX project InfectX (to UFG), and an Initial Training Networks grant (AdVance) from the European Union (to UFG).

References

1. **Mercer, J, M Schelhaas, and A Helenius.** 2010. Virus entry by endocytosis. Annu Rev Biochem **79:**803-833.

2. **Plemper, RK.** 2011. Cell entry of enveloped viruses. Current opinion in virology **1:**92-100.

3. **Grove, J, and M Marsh.** 2011. The cell biology of receptor-mediated virus entry. J Cell Biol **195:**1071-1082.

4. **Mercer, J, and UF Greber.** 2013. Virus interactions with endocytic pathways in macrophages and dendritic cells. Trends Microbiol **21:**380-388.

5. **Barrow, E, AV Nicola, and J Liu.** 2013. Multiscale perspectives of virus entry via endocytosis. Virol J **10:**177.

6. **Goubau, D, S Deddouche, and ESC Reis.** 2013. Cytosolic sensing of viruses. Immunity **38:**855-869.

7. **Gurtler, C, and AG Bowie.** 2013. Innate immune detection of microbial nucleic acids. Trends Microbiol **10.1016/j.tim.2013.04.004**.

8. **Moyer, C, and G Nemerow.** 2011. Viral weapons of membrane destruction: Variable modes of membrane penetration by non-enveloped viruses. Curr Op Virol **1:**44-49.

9. **Suomalainen, M, and UF Greber.** 2013. Uncoating of non-enveloped viruses. Current opinion in virology **3:**27-33.

10. **Yakimovich, A, H Gumpert, CJ Burckhardt, VA Lutschg, A Jurgeit, IF Sbalzarini, and UF Greber.** 2012. Cell-free transmission of human adenovirus by passive mass transfer in cell culture simulated in a computer model. J Virol **86:**10123–10137.

11. **Harrach, B, M Benkö, G Both, M Brown, A Davison, M Echavarría, M Hess, M Jones, A Kajon, H Lehmkuhl, V Mautner, S Mittal, and G Wadell.** 2011. Adenoviridae - ninth report of the international committee on taxonomy of viruses, p. 125-141. *In* A King, M Adams, E Carstens, and E Lefkowitz (ed.), Virus taxonomy. Elsevier, Oxford.

12. **Liu, H, L Jin, SB Koh, I Atanasov, S Schein, L Wu, and ZH Zhou.** 2010. Atomic structure of human adenovirus by cryo-em reveals interactions among protein networks. Science **329:**1038-1043.

13. **Reddy, VS, SK Natchiar, PL Stewart, and GR Nemerow.** 2010. Crystal structure of human adenovirus at 3.5 a resolution. Science **329:**1071-1075.

14. **Greber, UF, P Webster, J Weber, and A Helenius.** 1996. The role of the adenovirus protease on virus entry into cells. EMBO J **15:**1766-1777.

15. **Greber, UF, M Willetts, P Webster, and A Helenius.** 1993. Stepwise dismantling of adenovirus 2 during entry into cells. Cell **75:**477-486.

16. **Imelli, N, Z Ruzsics, D Puntener, M Gastaldelli, and UF Greber.** 2009. Genetic reconstitution of the human adenovirus type 2 temperature-sensitive 1 mutant defective in endosomal escape. Virol J **6:**174.

17. **Burckhardt, CJ, and UF Greber.** 2009. Virus movements on the plasma membrane support infection and transmission between cells. PLoS Pathog **5:**e1000621.

18. **Bergelson, JM, JA Cunningham, G Droguett, EA Kurt-Jones, A Krithivas, JS Hong, MS Horwitz, RL Crowell, and RW Finberg.** 1997. Isolation of a common receptor for coxsackie b viruses and adenoviruses 2 and 5. Science **275:**1320-1323.

19. **Tomko, RP, R Xu, and L Philipson.** 1997. Hcar and mcar: The human and mouse cellular receptors for subgroup c adenoviruses and group b coxsackieviruses. Proc. Natl. Acad. Sci. USA **94:**3352-3356.

20. **Gastaldelli, M, N Imelli, K Boucke, B Amstutz, O Meier, and UF Greber.** 2008. Infectious adenovirus type 2 transport through early but not late endosomes. Traffic **9:**2265-2278.

21. **Li, E, D Stupack, GM Bokoch, and GR Nemerow.** 1998. Adenovirus endocytosis requires actin cytoskeleton reorganization mediated by rho family gtpases. J. Virol. **72:**8806-8812.

22. **Meier, O, K Boucke, SV Hammer, S Keller, RP Stidwill, S Hemmi, and UF Greber.** 2002. Adenovirus triggers macropinocytosis and endosomal leakage together with its clathrin-mediated uptake. J Cell Biol **158:**1119-1131.

23. **Wang, K, S Huang, A Kapoor-Munshi, and G Nemerow.** 1998. Adenovirus internalization and infection require dynamin. J Virol **72:**3455-3458.

24. **Wickham, TJ, P Mathias, DA Cheresh, and GR Nemerow.** 1993. Integrins alpha v beta 3 and alpha v beta 5 promote adenovirus internalization but not virus attachment. Cell **73:**309-319.

25. **Trinh, HV, G Lesage, V Chennamparampil, B Vollenweider, CJ Burckhardt, S Schauer, M Havenga, UF Greber, and S Hemmi.** 2012. Avidity binding of human adenovirus serotypes 3 and 7 to the membrane cofactor cd46 triggers infection. Journal of Virology **86:**1623-1637.

26. **Wang, H, ZY Li, Y Liu, J Persson, I Beyer, T Moller, D Koyuncu, MR Drescher, R Strauss, XB Zhang, JK Wahl, 3rd, N Urban, C Drescher, A Hemminki, P Fender, and A Lieber.** 2011. Desmoglein 2 is a receptor for adenovirus serotypes 3, 7, 11 and 14. Nature Medicine **17:**96-104.

27. **Amstutz, B, M Gastaldelli, S Kälin, N Imelli, K Boucke, E Wandeler, J Mercer, S Hemmi, and UF Greber.** 2008. Subversion of ctbp1 controlled macropinocytosis by human adenovirus serotype 3. EMBO J. **27:**956-966.

28. **Kalin, S, B Amstutz, M Gastaldelli, N Wolfrum, K Boucke, M Havenga, F DiGennaro, N Liska, S Hemmi, and UF Greber.** 2010. Macropinocytotic uptake and infection of human epithelial cells with species b2 adenovirus type 35. J Virol **84:**5336-5350.

29. **Miyasawa, N, RG Crystal, and PL Leopold.** 2001. Adenovirus serotype 7 retention in a late endosomal compartment prior to cytosol escape is modulated by fiber protein. J.Virol. **75:**1387-1400.

30. **Wiethoff, CM, H Wodrich, L Gerace, and GR Nemerow.** 2005. Adenovirus protein vi mediates membrane disruption following capsid disassembly. J Virol **79:**1992-2000.

31. **Moyer, CL, CM Wiethoff, O Maier, JG Smith, and GR Nemerow.** 2011. Functional genetic and biophysical analyses of membrane disruption by human adenovirus. J Virol **85:**2631-2641.

32. **Burckhardt, CJ, M Suomalainen, P Schoenenberger, K Boucke, S Hemmi, and UF Greber.** 2011. Drifting motions of the adenovirus receptor car and immobile integrins initiate virus uncoating and membrane lytic protein exposure. Cell Host Microbe **10:**105-117.

33. **Brabec, M, D Schober, E Wagner, N Bayer, RF Murphy, D Blaas, and R Fuchs.** 2005. Opening of size-selective pores in endosomes during human rhinovirus serotype 2 in vivo uncoating monitored by single-organelle flow analysis. J Virol **79:**1008-1016.

34. **Farr, GA, LG Zhang, and P Tattersall.** 2005. Parvoviral virions deploy a capsid-tethered lipolytic enzyme to breach the endosomal membrane during cell entry. Proc Natl Acad Sci U S A **102:**17148-17153.

35. **Seth, P, DJ Fitzgerald, MC Willingham, and I Pastan.** 1984. Role of a low-ph environment in adenovirus enhancement of the toxicity of a pseudomonas exotoxin-epidermal growth factor conjugate. J. Virol. **51:**650-655.

36. **Maier, O, DL Galan, H Wodrich, and CM Wiethoff.** 2010. An n-terminal domain of adenovirus protein vi fragments membranes by inducing positive membrane curvature. Virology **402** 11-19.

37. **Moyer, CL, and GR Nemerow.** 2012. Disulfide-bond formation by a single cysteine mutation in adenovirus protein vi impairs capsid release and membrane lysis. Virology **428:**41-47.

38. **Perez-Berna, AJ, R Marabini, SH Scheres, R Menendez-Conejero, IP Dmitriev, DT Curiel, WF Mangel, SJ Flint, and C San Martin.** 2009. Structure and uncoating of immature adenovirus. J Mol Biol **392:**547-557.

39. **Laver, WG, NG Wrigley, and HG Pereira.** 1969. Removal of penton from particles of adenovirus type 2. Virology **39:**599-605.

40. **Horne, WS, CM Wiethoff, C Cui, KM Wilcoxen, M Amorin, MR Ghadiri, and GR Nemerow.** 2005. Antiviral cyclic d,l-alpha-peptides: Targeting a general biochemical pathway in virus infections. Bioorg Med Chem **13:**5145-5153.

41. **Blumenthal, R, P Seth, MC Willingham, and I Pastan.** 1986. Ph-dependent lysis of liposomes by adenovirus. Biochemistry **25:**2231-2237.

42. **Pastan, I, P Seth, D FitzGerald, and M Willingham.** 1986. Adenovirus entry into cells: Some new observations on an old problem. Springer Verlag, New York.

43. **Jurgeit, A, S Moese, P Roulin, A Dorsch, M Lotzerich, WM Lee, and UF Greber.** 2010. An rna replication-center assay for high content image-based quantifications of human rhinovirus and coxsackievirus infections. Virol J **7:**264.

44. **Greber, UF, MY Nakano, and M Suomalainen.** 1998. Adenovirus entry into cells: A quantitative fluorescence microscopy approach, p. 217-230. *In* WSM Wold (ed.), Adenovirus methods and protocols, in meth. Mol. Med. Vol 21. Humana Press, Inc, Totowa, NJ USA.

45. **Nagel, H, S Maag, A Tassis, FO Nestle, UF Greber, and S Hemmi.** 2003. The alphavbeta5 integrin of hematopoietic and nonhematopoietic cells is a transduction receptor of rgd-4c fiber-modified adenoviruses. Gene Ther **10:**1643-1653.

46. **Fleischli, C, D Sirena, G Lesage, MJ Havenga, R Cattaneo, UF Greber, and S Hemmi.** 2007. Species b adenovirus serotypes 3, 7, 11 and 35 share similar binding sites on the membrane cofactor protein cd46 receptor. J Gen Virol **88:**2925-2934.

47. **Sirena, D, Z Ruzsics, W Schaffner, UF Greber, and S Hemmi.** 2005. The nucleotide sequence and a first generation gene transfer vector of species b human adenovirus serotype 3. Virology **343:**283-298.

48. **Suomalainen, M, MY Nakano, K Boucke, S Keller, RP Stidwill, and UF Greber.** 1999. Microtubule-dependent minus and plus end-directed motilities are competing processes for nuclear targeting of adenovirus. J. Cell Biol. **144:**657-672.

49. **Puntener, D, MF Engelke, Z Ruzsics, S Strunze, C Wilhelm, and UF Greber.** 2011. Stepwise loss of fluorescent core protein v from human adenovirus during entry into cells. J Virol **85:**481-496.

50. **Varghese, R, Y Mikyas, PL Stewart, and R Ralston.** 2004. Postentry neutralization of adenovirus type 5 by an antihexon antibody. J Virol **78:**12320-12332.

51. **Jurgeit, A, R McDowell, S Moese, E Meldrum, R Schwendener, and UF Greber.** 2012. Niclosamide is a proton carrier and targets acidic endosomes with broad antiviral effects. PLoS Pathog **8:**e1002976.

52. **Lutschg, V, K Boucke, S Hemmi, and UF Greber.** 2011. Chemotactic anti-viral cytokines promote infectious apical entry of human adenovirus into polarized epithelial cells, p. 391, Nat Commun, vol. 2. Nature Publishing Group.

53. **Walkiewicz, MP, N Morral, and DA Engel.** 2009. Accurate single-day titration of adenovirus vectors based on equivalence of protein vii nuclear dots and infectious particles. J Virol Methods **159:**251-258.

54. **Walev, I, SC Bhakdi, F Hofmann, N Djonder, A Valeva, K Aktories, and S Bhakdi.** 2001. Delivery of proteins into living cells by reversible membrane permeabilization with streptolysin-o. Proc Natl Acad Sci USA **98:**3185-3190.

55. **Bowman, EJ, A Siebers, and K Altendorf.** 1988. Bafilomycins: A class of inhibitors of membrane atpases from microorganisms, animal cells, and plant cells. Proc Natl Acad Sci U S A **85:**7972-7976.

56. **Poole, B, and S Ohkuma.** 1981. Effect of weak bases on the intralysosomal ph in mouse peritoneal macrophages. J Cell Biol **90:**665-669.

57. **Helenius, A, M Marsh, and J White.** 1982. Inhibition of semliki forest virus penetration by lysosomotropic weak bases. J. Gen. Virol. **58:**47-61.

58. **Greber, UF, M Suomalainen, RP Stidwill, K Boucke, M Ebersold, and A Helenius.** 1997. The role of the nuclear pore complex in adenovirus DNA entry. EMBO J. **16:**5998-6007.

59. **Perez, L, and L Carrasco.** 1994. Involvement of the vacuolar h(+)-atpase in animal virus entry. J. Gen. Virol. **75:**2595-2606.

60. **Zeng, X, and CR Carlin.** 2013. Host cell autophagy modulates early stages of adenovirus infections in airway epithelial cells. J Virol **87:**2307-2319.

61. **Nakano, MY, K Boucke, M Suomalainen, RP Stidwill, and UF Greber.** 2000. The first step of adenovirus type 2 disassembly occurs at the cell surface, independently of endocytosis and escape to the cytosol. J Virol **74:**7085-7095.

62. **Seth, P, MC Willingham, and I Pastan.** 1984. Adenovirus-dependent release of ^{51}cr from kb cells at an acidic ph. J. Biol. Chem. **259:**14350-14353.

63. **Wickham, TJ, EJ Filardo, DA Cheresh, and GR Nemerow.** 1994. Integrin avb5 selectively promotes adenovirus mediated cell membrane permeabilization. J Cell Biol **127:**257-264.

64. **Wang, I, M Suomalainen, V Andriasyan, S Kilcher, J Mercer, A Neef, N Luedtke, and UF Greber.** 2013. Tracking viral genomes in host cells at single molecule resolution by click chemistry and super-resolution microscopy. Cell Host & Microbe **in press**.

Figure legends

Fig. 1: SLO-mediated perforation of the plasma membrane allows quantification of cytosolic and endosomal viruses

(A) Protocol and graphical representation of the assay measuring virus penetration into the cytosol of cultured cells. Plasma membrane-associated and cytosolic viruses are detected in green by Alexa Fluor 488 (Alexa-488) plus red (Alexa-594) colors, whereas endosomal viruses are exclusively green (Alexa-488).

(B) Alexa-488-labeled HAdV-C2 wild type (wt), but not the penetration-deficient Alexa-488-labeled TS1 particles are accessible to anti-Alexa-488 antibodies in SLO-treated HeLa-Ohio cells 30 min after internalization. Images shown represent maximum projections of individual confocal stacks. In the merge image Alexa-488 and Alexa-594 double positive particles are yellow. Nuclei (DAPI stain) are blue. Scale bar = 10 µm.

(C) Quantification of surface and cytosolic viruses in cells infected with wt Alexa-488-labeled HAdV-C5. Intact cells were stained with both the mouse anti-hexon 9C12 and rabbit anti-Alexa-488 antibodies at 0 min, whereas at other time points intact cells were first incubated with the 9C12 antibody, then SLO-treated and incubated with anti-Alexa-488 antibodies. Primary antibodies were detected by secondary Alexa-594-conjugated anti-mouse and Alexa-633-conjugated anti-rabbit antibodies. The plot shows percentage of virus particles positive for 9C12 (9C; these particles represent surface particles) and particles positive for anti-Alexa-488 antibody, but negative for 9C12 (AI; these particles represent cytosolic particles). One dot represents one cell. Error bars represent the mean ± SEM. Numbers of cells and viruses analyzed are indicated.

(D) Quantification of anti-Alexa-488 positive particles in cells infected with Alexa-488-labeled TS1. In SLO(-) samples, intact cells were stained with the antibody to estimate the number of viruses at the plasma membrane, whereas the parallel SLO(+) sample indicates the number of antibody positive particles in SLO-treated cells. Difference between SLO(-) and SLO(+) samples represents the cytosolic virus population. TX-100 sample is an SLO-treated sample that was fixed and permeabilised with TX-100 before staining with anti-Alexa-488 antibodies. Error bars represent the mean ± SEM. Numbers of cells and viruses analyzed are indicated.

(E) The majority of Alexa-488-labeled TS1 particles are endosomal in cells co-infected with wt and TS1 viruses. Unlabeled wt HAdV-C5 and Alexa-488-labeled TS1 were co-internalized into the cells for 30 min before SLO treatment. Control cells were infected with Alexa-488-labeled TS1 alone. The SLO-permeabilised cells were incubated with mouse 9C12 anti-hexon and rabbit anti-Alexa-488 antibodies at cold, fixed and treated with Alexa-680-conjugated anti-mouse and Alexa-594-conjugated anti-rabbit antibodies and DAPI. The right hand fluorograph shows that wt particles in the wt and TS1 co-infected cells were readily accessible to the anti-hexon antibody. The left hand panel shows the percentage of TS1 particles positive for anti-Alexa-488 antibody in the TS1 single and the TS1 plus wt double infection (one dot represents one cell). The difference between TS1 single and wt and TS1 double infection was statistically highly significant (two-tailed Mann-Whitney test).

Fig. 2: Penetration of HAdV-C2 in A549 cells is rapid and efficient

(A) The majority of Alexa-488-labeled wt HAdV-C2 (upper panel), but not the Alexa-488-labeled TS1 particles are accessible to anti-Alexa-488 antibodies in SLO-treated A549 cells 20 min after internalization. The experiment was done as described in legend to Fig. 1. Images shown represent maximum projections of individual confocal stacks. In the merge image, Alexa-488 and Alexa-594 double positive particles are yellow. Nuclei (DAPI stain) are blue. Scale bar = 10 µm.

(B) Quantification of anti-Alexa-488 positive wt and TS1 particles in intact (SLO / -) or parallel SLO-permeabilized A549 cells (SLO / +) at 20 min post internalization (one dot represents one cell). Error bars represent the mean ± SEM. Numbers of cells and viruses analyzed are indicated.

Fig. 3: Acidic endosomal pH is not required for efficient penetration of HAdV-C2

(A) Bafilomycin A1 (Baf A1, 50 nM), niclosamide (5 µM) and NH_4Cl (25 mM) efficiently neutralize acidic compartments. HeLa-Ohio cells were treated with the indicated concentrations of the drugs for 60 min, incubated with DND-99 lysotracker

(red) to stain acidic compartments, fixed and stained with Hoechst dye (blue), and analyzed by confocal microscopy. Control cells for Baf A1 and niclosamide were treated with dmso, and the control for NH_4Cl was pH 8.2 culture medium. Images shown represent maximum projections of individual stacks (DND-99) or a single confocal section (Hoechst). Scale bar = 10 µm.

(B) Penetration efficiency of HAdV-C2 in Baf A1-treated cells. Cells were permeabilised with SLO 20 min after virus internalization. The plot shows percentage of virus particles positive for the anti-Alexa-488 antibody (one dot represents one cell). Error bars represent the mean ± SEM. Numbers of cells and viruses analyzed are indicated.

(C) Penetration efficiency in niclosamide-treated cells. Cells were permeabilised with SLO at 60 min post virus internalization. Differences between control and niclosamide-treated samples in the wt infection were statistically highly significant (two-tailed Mann-Whitney test).

(D) Penetration efficiency in NH_4Cl-treated cells. Cells were permeabilised with SLO at 30 min post virus internalization. Although differences between control and NH_4Cl-treated cells in the wt infection were statistically highly significant, only in minority of NH_4Cl-treated cells the wt virus penetration efficiency was similar to that of TS1.

(E) Two representative transmission electron micrographs of control cells 30 min pi, showing three cytoplasmic HAdV-C2 (upper panel, arrowheads) and an endosomal virus (lower panel, arrow). Scale bar 200 nm.

(F) Quantification of HAdV-C2 particles in the cytosol of DMSO control cells, Baf A1 or niclosamide-treated cells 30 min pi, as percent of total particles associated with the cells based on transmission EM analyses. One dot represents one cell.

Fig. 4: Neutralization of endosomal pH does not inhibit exposure of the viral membrane lytic protein VI

(A) Immunofluorescence labeling of protein VI (green) in HeLa-Ohio cells infected with Ad5-atto-565 (red). Ad5-atto-565 was bound to cells at cold and internalized at 37°C for 0 min or 10 min. Cells were fixed and stained for protein VI. Images

represent maximum projections of individual stacks. The protein VI-positive particles in the merge image are shown in yellow, and nuclei (DAPI) in blue. Scale bar = 10 µm.

(B) Protein VI exposure in infected Baf A1-treated cells. The cells were pretreated with dmso or the drug for 60 min, atto-565-labeled Ad5-wt particles were bound to cells at cold and internalized for the indicated times in the presence of dmso/drug. Intact cells were first stained with mouse anti-hexon 9C12 antibody on ice to tag surface particles, fixed, permeabilised with Triton X-100 and stained with rabbit anti-protein VI antibodies. Secondary Alexa-680-conjugated anti-mouse and Alexa-488-conjugated anti-rabbit antibodies were used to detect the 9C12 and anti-protein VI antibodies, respectively. Nuclei were stained with DAPI. Samples were imaged by confocal microscopy and images from maximum projections of confocal stacks were analyzed by a custom programmed MatLab routine to quantitate the Alexa-488-signal on endocytosed virus particles (atto-565-positive, but Alexa-680-negative viruses). The plot shows mean fluorescent protein VI signal on endocytosed particles (arbitrary units: one dot represents the mean value from one cell). Error bars represent the mean ± SEM. Protein VI signal on endocytosed viruses in Baf A1-treated cells was slightly, but statistically significantly, higher than that in control cells at 10 min post virus internalization (two-tailed Mann-Whitney test). Numbers of cells and viruses analyzed are indicated. Protein VI separates from virus particles after penetration, which is indicated by the reduced protein VI signal on viruses 20 min post-internalization.

(C) Protein VI exposure in infected, niclosamide-treated HeLa-Ohio cells. The experiment was carried out as in (B).

(D) Protein VI exposure in infected, NH_4Cl-treated HeLa-Ohio cells. The experiment was carried out as in (B).

Fig. 5: Nuclear delivery of incoming viral DNA associated protein VII and viral transgene expression are not inhibited by low pH-neutralization

(A) Dmso and Baf A1 treated cells bind similar amounts of virus. HeLa-Ohio cells were pretreated with dmso or 50 nM BAFA1 for 1h. HAdV-C5 was bound to cells at

37°C for 30 min in the presence of dmso/Baf A1. Unbound virus was washed away, cells were fixed and immunostained with anti-hexon 9C12 antibody and DAPI for nucleus. Samples were imaged by confocal microscopy, and analyzed by custom programmed MatLab routine. The plot shows number of viruses per cell (one dot represents one cell). The error bar represents the mean ± SEM. Number of cells and viruses analyzed are indicated. The differences between dmso and BAFA1 samples were not statistically significant.

(B) Immunofluorescence labeling of protein VII in HeLa-Ohio cells infected with HAdV-C5 for 3 h. Images shown represent maximum projections of confocal stacks (protein VII, green) or a single confocal section (DAPI, blue). Incoming protein VII is seen as discreet dots over the nuclear area. Staining of non-infected cells is shown as a control for signal specificity. Scale bar = 10 µm.

(C) Quantification of nuclear protein VII dots at 3 h post virus internalization indicates that nuclear import of protein VII occurs as efficiently in Baf A1-treated cells as in control cells. Error bars represent the mean ± SEM. The number of nuclei analyzed is shown below the plot. Comparison of samples infected with 60 ng or 30 ng of virus indicate that the number of nuclear protein VII dots correlates with input virus.

(D) Baf A1 boosts HAdV-C5_GFP infection. Cells were pretreated with dmso or Baf A1 for 60 min, a non-replicating HAdV-C5_GFP reporter virus was bound to cells for 30 min at 37°C and the cells were further incubated at 37°C for 17 h in the presence of dmso/Baf A1 (-60min sample). Alternatively, dmso/Baf A1 was added 2 h after virus binding (+120min sample). Cells were fixed, stained with DAPI, and imaged by automated fluorescence microscopy. The average intensity of EGFP over a DAPI mask was quantitated by a custom programmed MatLab routine. The effect of the drug treatment on cell viability (estimated by cell adhesion) is indicated by the cell number. The values represent mean values from three parallel samples ±SD. Since Bafilomycin A1 boosted infection efficiency even when added 2 h after virus binding, the boost is not connected to penetration.

(E) Niclosamide slightly reduces the infection efficiency. HeLa-Ohio cells were pretreated with dmso/drug for 60 min. Virus was bound to cells at 37°C for 30 min and cells were further incubated at 37°C for 3.5 h in the presence of

dmso/niclosamide, followed by 14.5 h incubation in drug-free medium. The samples were processed as described in (D).

Fig. 6: Efficiency of HAdV-B3 penetration and infection in Baf A1- and niclosamide-treated cells

(A) SLO-mediated perforation of the plasma membrane allows detection of cytosolic but not endosomal virus population in HAdV-B3-infected cells. Alexa-488 (Alexa488)-labeled HAdV-B3 was bound to HeLa-Ohio cells at cold and internalized at 37°C for 30 min before SLO-permeabilization of cells. The samples were processed and analyzed as described in Fig. 1A. Images represent maximum projections of individual stacks. In the merge image cytosolic virus is yellow. Nuclei (DAPI signal) are blue. Scale bar = 10 µm.

(B) Time course of HAdV-B3 penetration.

(C) Baf A1 does not inhibit penetration of HAdV-B3. Cells were pretreated with dmso or Baf A1 for 1 h, Alexa-488-labeled virus was bound to cells at cold and internalized at 37°C for 1 h in presence of dmso/drug before SLO-permeabilization. SLO(-)-sample represents intact cells treated with anti-Alexa-488 antibody at cold to detect surface particles. The plot shows percentage of virus particles positive for the anti-Alexa-488 antibody (one dot represents one cell). Error bars represent the mean ± SEM. Number of cells and viruses analyzed are indicated.

(D) Niclosamide slightly, but statistically significantly, reduces the penetration of HAdV-B3. The experiment was done as described in (C). Two-tailed Mann-Whitney test was used for statistical analyses.

(E) Baf A1 boosts the infection efficiency. The experiment was carried out as described in legend to Fig. 5D, except that cells were fixed 18 h after removal of virus inoculum. In contrast to HAdV-C5_EGFP, late addition of the drug significantly reduced the infection boost.

(F) Niclosamide boosts the infection efficiency. The experiment was carried out as described in legend to Fig. 5E, except that cells were fixed 13 h after drug removal.

F1

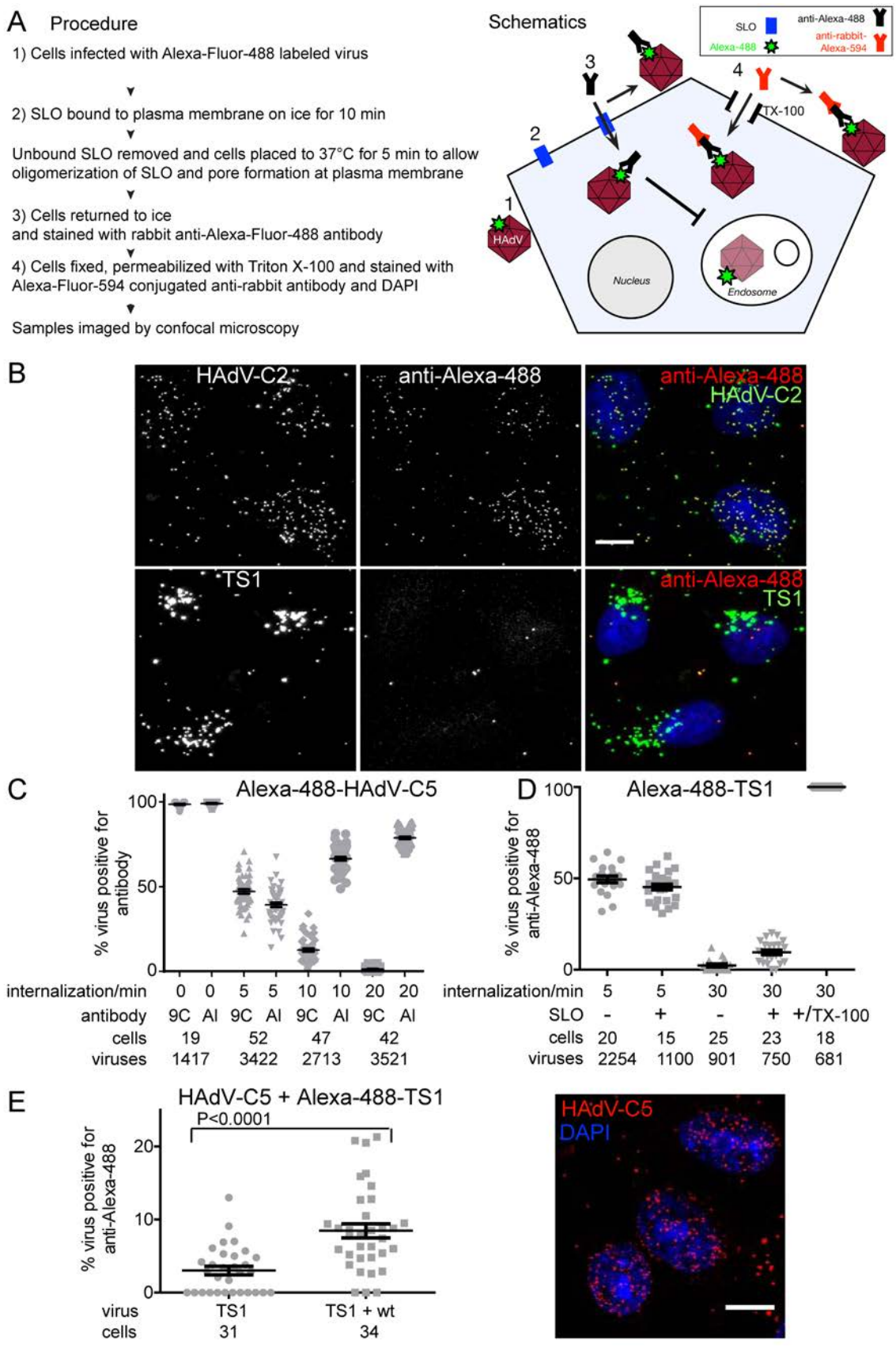
A Procedure
1) Cells infected with Alexa-Fluor-488 labeled virus
2) SLO bound to plasma membrane on ice for 10 min
Unbound SLO removed and cells placed to 37°C for 5 min to allow oligomerization of SLO and pore formation at plasma membrane
3) Cells returned to ice and stained with rabbit anti-Alexa-Fluor-488 antibody
4) Cells fixed, permeabilized with Triton X-100 and stained with Alexa-Fluor-594 conjugated anti-rabbit antibody and DAPI
Samples imaged by confocal microscopy
Schematics
SLO
Alexa-488
anti-Alexa-488
anti-rabbit-Alexa-594
TX-100
HAdV
Nucleus
Endosome
B
HAdV-C2
anti-Alexa-488
anti-Alexa-488 HAdV-C2
TS1
anti-Alexa-488 TS1
C
Alexa-488-HAdV-C5
% virus positive for antibody
internalization/min 0 0 5 5 10 10 20 20
antibody 9C AI 9C AI 9C AI 9C AI
cells 19 52 47 42
viruses 1417 3422 2713 3521
D
Alexa-488-TS1
% virus positive for anti-Alexa-488
internalization/min 5 5 30 30 30
SLO - + - + +/TX-100
cells 20 15 25 23 18
viruses 2254 1100 901 750 681
E
HAdV-C5 + Alexa-488-TS1
P<0.0001
% virus positive for anti-Alexa-488
virus TS1 TS1 + wt
cells 31 34
HAdV-C5
DAPI

F2

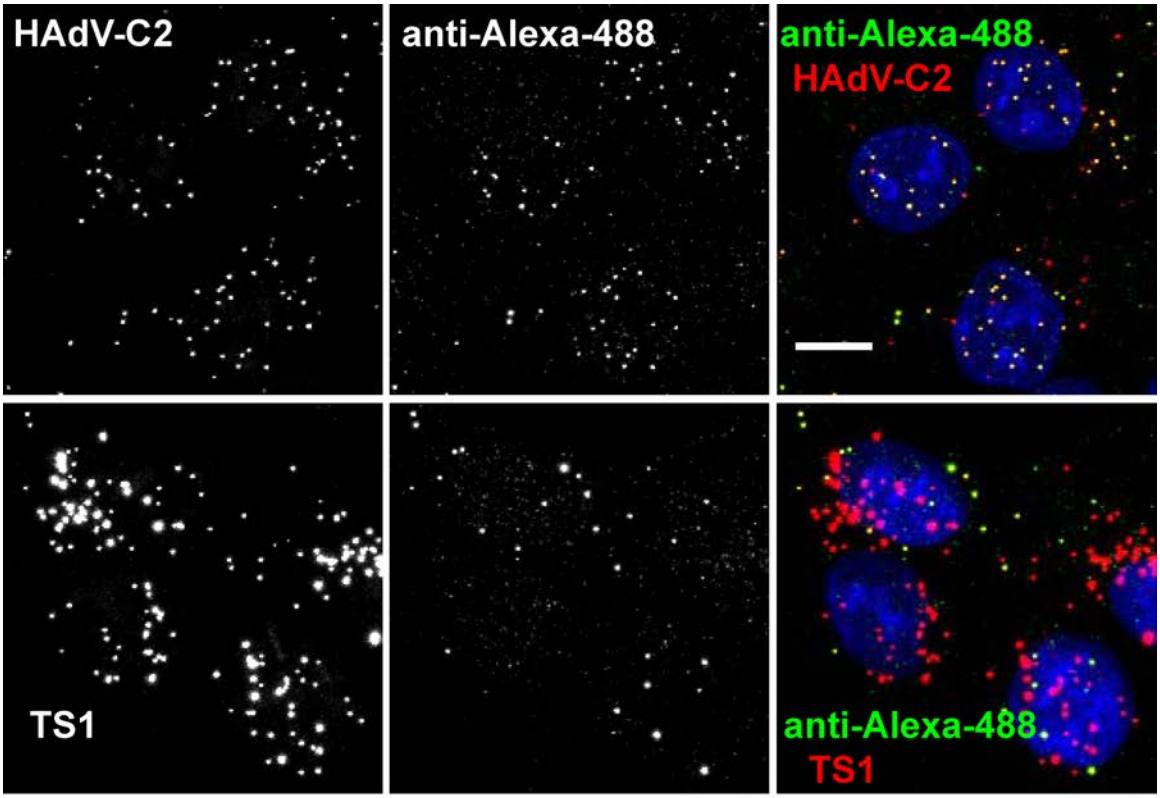
HAdV-C2
anti-Alexa-488
anti-Alexa-488
HAdV-C2
TS1
anti-Alexa-488
TS1

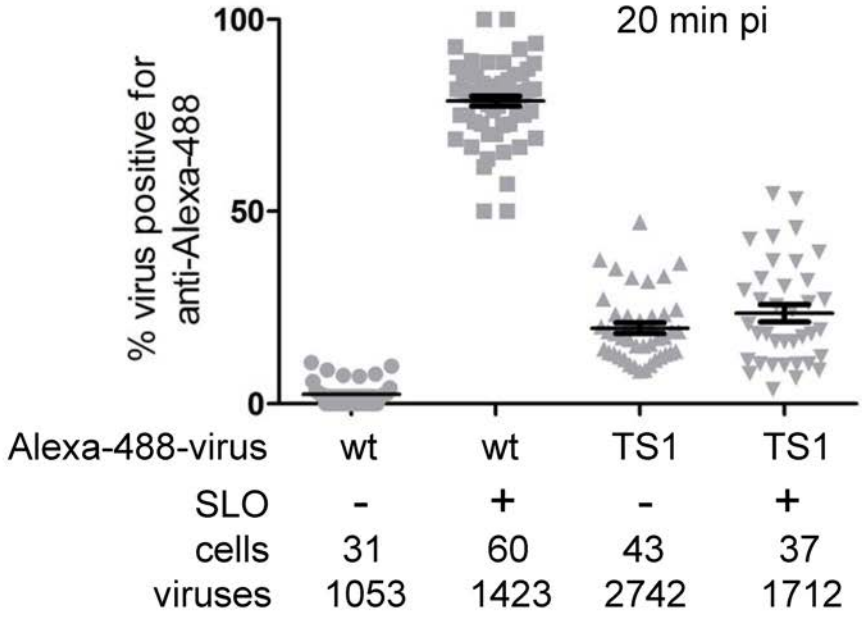
20 min pi
% virus positive for anti-Alexa-488
100
50
0
Alexa-488-virus wt wt TS1 TS1
SLO - + - +
cells 31 60 43 37
viruses 1053 1423 2742 1712

F3

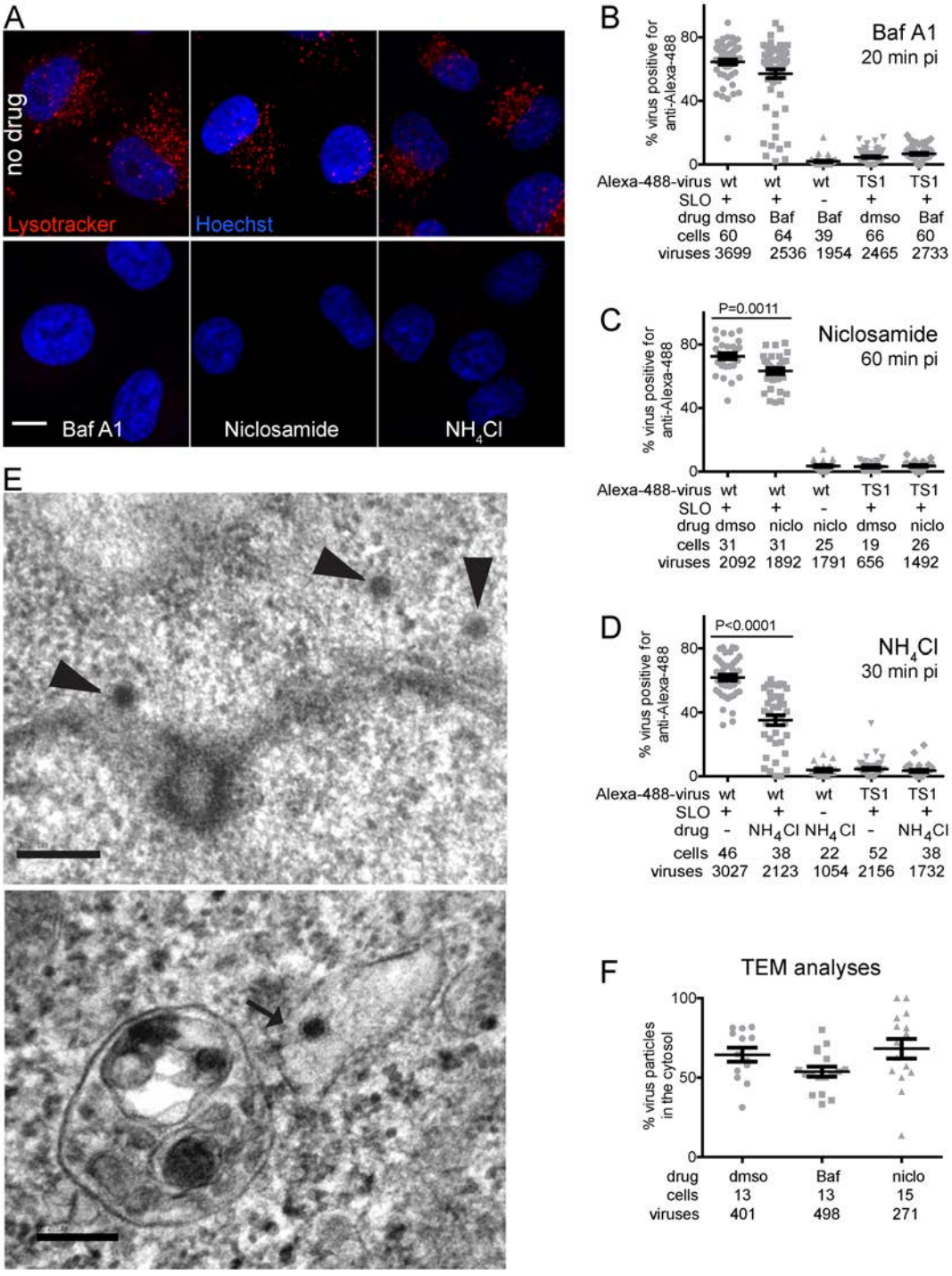
A
no drug
Lysotracker
Hoechst
Baf A1
Niclosamide
NH4Cl
B
Baf A1
20 min pi
% virus positive for anti-Alexa-488
Alexa-488-virus wt wt wt TS1 TS1
SLO + + - + +
drug dmso Baf Baf dmso Baf
cells 60 64 39 66 60
viruses 3699 2536 1954 2465 2733
C
P=0.0011
Niclosamide
60 min pi
% virus positive for anti-Alexa-488
Alexa-488-virus wt wt wt TS1 TS1
SLO + + - + +
drug dmso niclo niclo dmso niclo
cells 31 31 25 19 26
viruses 2092 1892 1791 656 1492
D
P<0.0001
NH4Cl
30 min pi
% virus positive for anti-Alexa-488
Alexa-488-virus wt wt wt TS1 TS1
SLO + + - + +
drug - NH4Cl NH4Cl - NH4Cl
cells 46 38 22 52 38
viruses 3027 2123 1054 2156 1732
E
F
TEM analyses
% virus particles in the cytosol
drug dmso Baf niclo
cells 13 13 15
viruses 401 498 271

F4

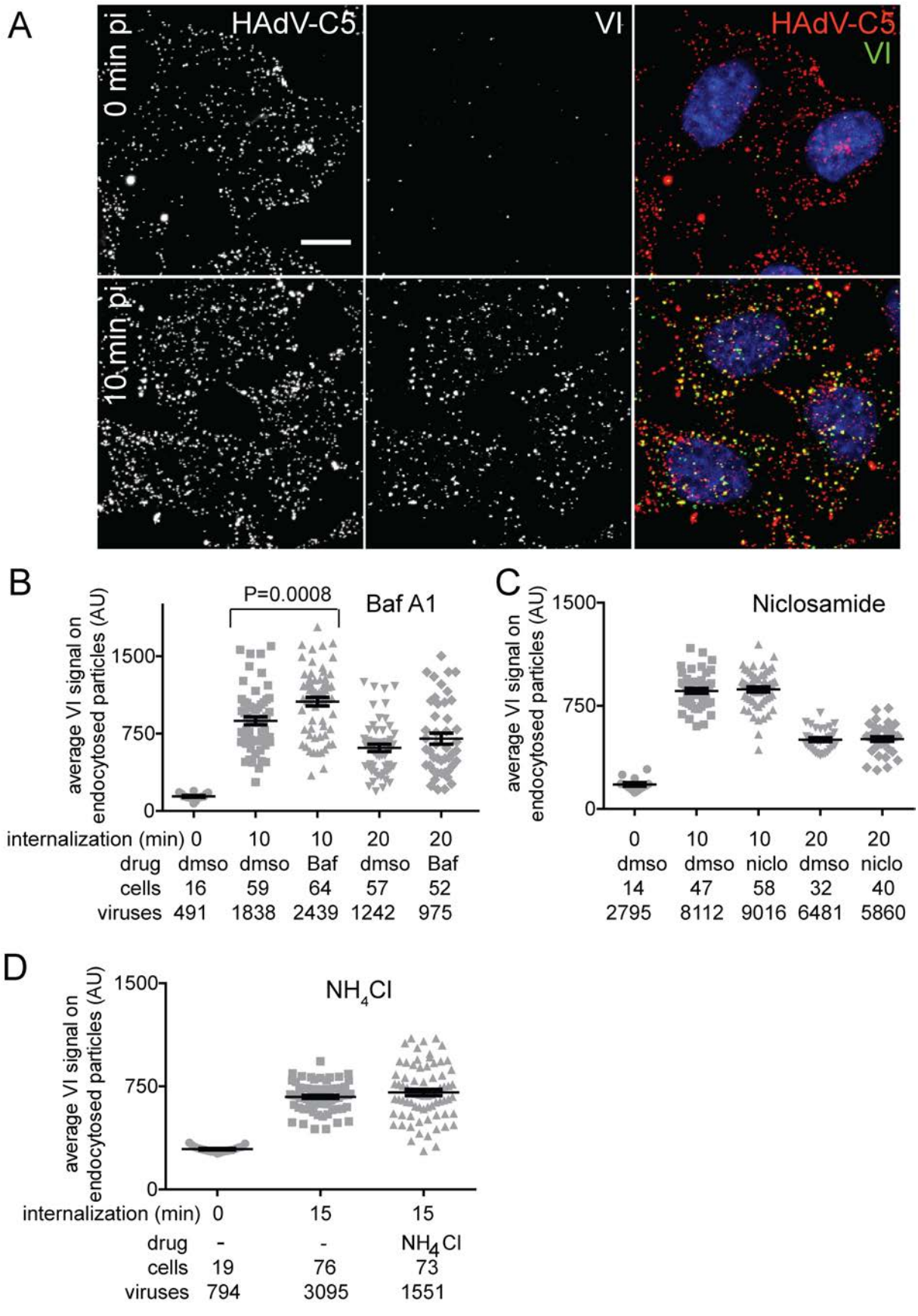
A
HAdV-C5
VI
HAdV-C5
VI
0 min pi
10 min pi
B
P=0.0008
Baf A1
average VI signal on endocytosed particles (AU)
1500
750
0
internalization (min) 0 10 10 20 20
drug dmso dmso Baf dmso Baf
cells 16 59 64 57 52
viruses 491 1838 2439 1242 975
C
Niclosamide
average VI signal on endocytosed particles (AU)
1500
750
0
0 10 10 20 20
dmso dmso niclo dmso niclo
14 47 58 32 40
2795 8112 9016 6481 5860
D
NH4Cl
average VI signal on endocytosed particles (AU)
1500
750
0
internalization (min) 0 15 15
drug - - NH4Cl
cells 19 76 73
viruses 794 3095 1551

F5

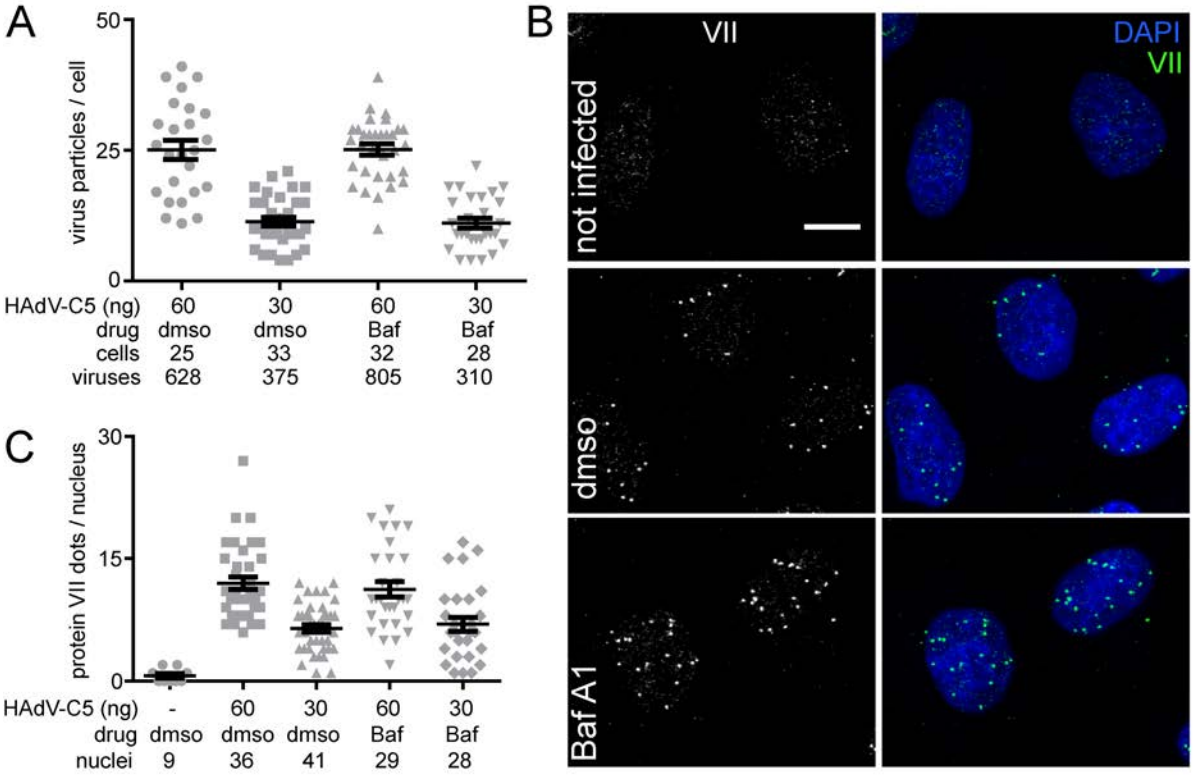
A
virus particles / cell
50
25
0
HAdV-C5 (ng) 60 30 60 30
drug dmso dmso Baf Baf
cells 25 33 32 28
viruses 628 375 805 310
B
VII
DAPI
VII
not infected
dmso
Baf A1
C
protein VII dots / nucleus
30
15
0
HAdV-C5 (ng) - 60 30 60 30
drug dmso dmso dmso Baf Baf
nuclei 9 36 41 29 28

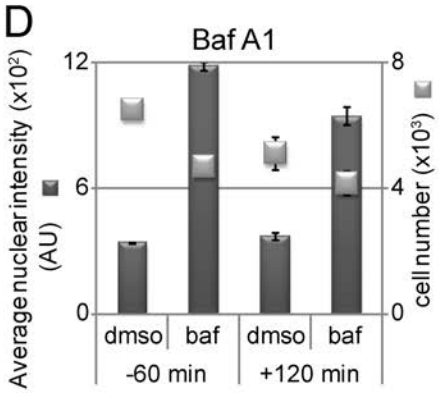
D
Baf A1
Average nuclear intensity (x10²) (AU)
cell number (x10³)
12
6
0
8
4
0
dmso
baf
dmso
baf
-60 min
+120 min

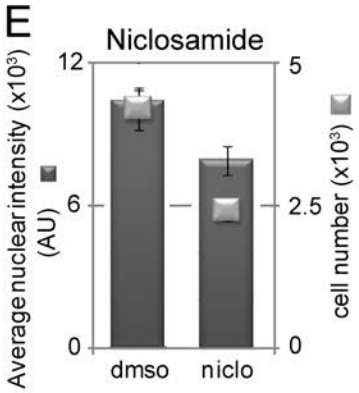
E
Niclosamide
Average nuclear intensity (x10³) (AU)
cell number (x10³)
12
6
0
5
2.5
0
dmso
niclo

F6

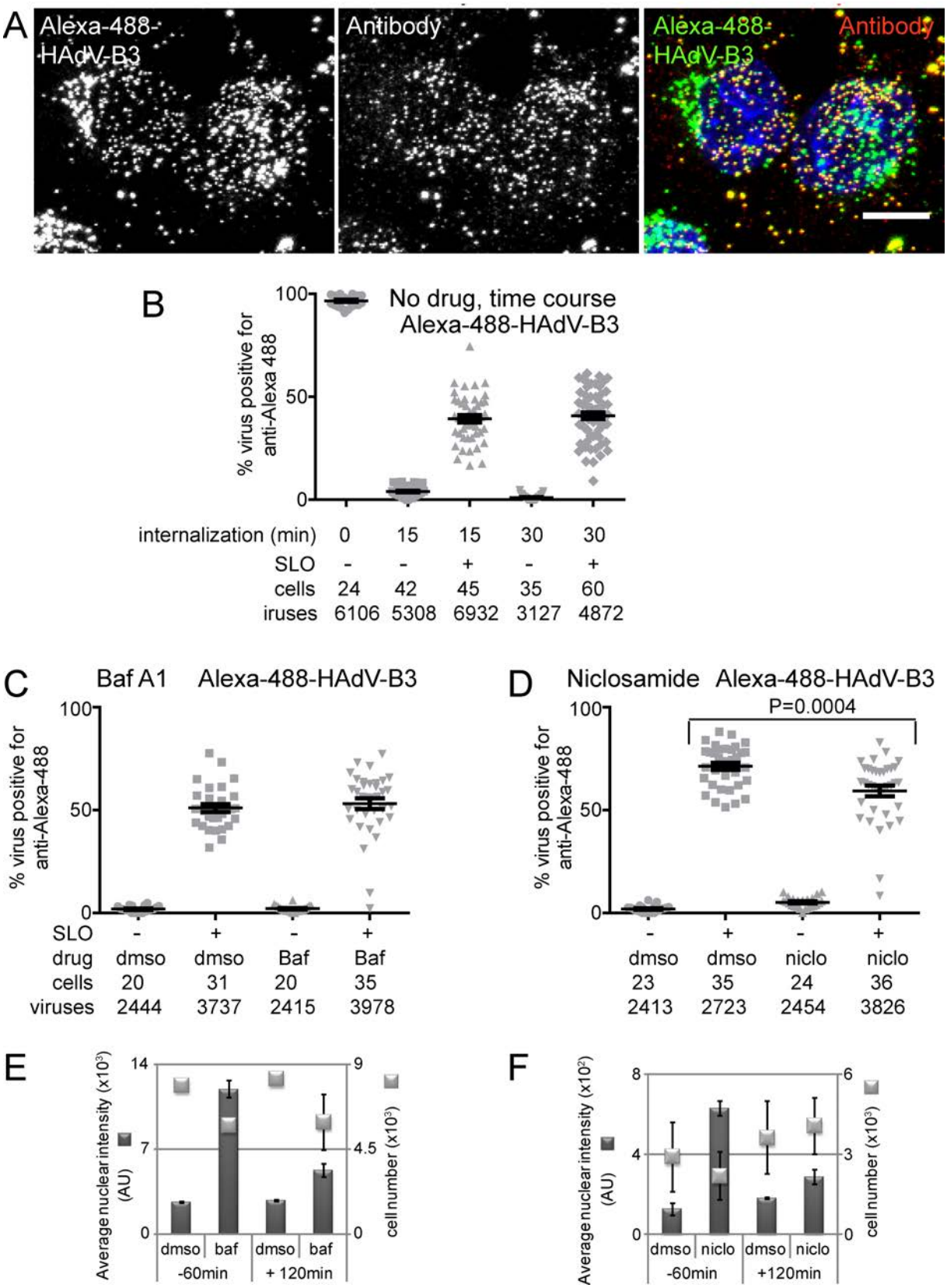
A
Alexa-488-HAdV-B3
Antibody
Alexa-488-HAdV-B3
Antibody
B
No drug, time course
Alexa-488-HAdV-B3
% virus positive for anti-Alexa 488
100
50
0
internalization (min) 0 15 15 30 30
SLO - - + - +
cells 24 42 45 35 60
iruses 6106 5308 6932 3127 4872
C
Baf A1 Alexa-488-HAdV-B3
% virus positive for anti-Alexa-488
100
50
0
SLO - + - +
drug dmso dmso Baf Baf
cells 20 31 20 35
viruses 2444 3737 2415 3978
D
Niclosamide Alexa-488-HAdV-B3
P=0.0004
% virus positive for anti-Alexa-488
100
50
0
- + - +
dmso dmso niclo niclo
23 35 24 36
2413 2723 2454 3826
E
Average nuclear intensity (x10³) (AU)
14
7
0
9
4.5
0
cell number (x10³)
dmso baf dmso baf
-60min + 120min
F
Average nuclear intensity (x10²) (AU)
8
4
0
6
3
0
cell number (x10³)
dmso niclo dmso niclo
-60min +120min